Probing mesoscopic crystals with electrons: One-step simultaneous inelastic and elastic scattering theory

Vladimir U. Nazarov*
Research Center for Applied Sciences, Academia Sinica, Taipei 11529, Taiwan

Vyacheslav M. Silkin and Eugene E. Krasovskii
Departamento de Física de Materiales, Facultad de Ciencias Quíimicas, Universidad del Pais Vasco/Euskal Herriko Unibertsitatea, Apdo. 1072, San Sebastián/Donostia, 20080 Basque Country, Spain;
Donostia International Physics Center (DIPC), Paseo Manuel de Lardizabal 4, San Sebastián/Donostia, 20018 Basque Country, Spain and IKERBASQUE, Basque Foundation for Science, 48013 Bilbao, Spain

(Received 3 August 2017; revised manuscript received 7 November 2017; published 11 December 2017)

Inelastic scattering of the medium-energy (∼10–100 eV) electrons underlies the method of the high-resolution electron energy-loss spectroscopy (HREELS), which has been successfully used for decades to characterize pure and adsorbate-covered surfaces of solids. With the emergence of graphene and other quasi-two-dimensional (Q2D) crystals, HREELS could be expected to become the major experimental tool to study this class of materials. We, however, identify a critical flaw in the theoretical picture of the HREELS of Q2D crystals in the context of the inelastic scattering only ("energy-loss functions" formalism), in contrast to its justifiable use for bulk solids and surfaces. The shortcoming is the neglect of the *elastic* scattering, which we show is inseparable from the inelastic one, and which, affecting the spectra dramatically, must be taken into account for the meaningful interpretation of the experiment. With this motivation, using the time-dependent density functional theory for excitations, we build a theory of the simultaneous inelastic and elastic electron scattering at Q2D crystals. We apply this theory to HREELS of graphene, revealing an effect of the strongly coupled excitation of the $\pi + \sigma$ plasmon and elastic *diffraction resonances*. Our results open a path to the theoretically interpretable study of the excitation processes in crystalline mesoscopic materials by means of HREELS, with its supreme resolution on the meV energy scale, which is far beyond the capacity of the now overwhelmingly used EELS in transmission electron microscopy.

DOI: 10.1103/PhysRevB.96.235414

I. INTRODUCTION

While electron energy-loss spectroscopy (EELS) is a powerful experimental tool in the studies of the growing family of quasi-two-dimensional (Q2D) materials, its theoretical support for these systems remains unsatisfactory, being based on, often irrelevant, analogies with the bulks and surfaces of the three-dimensional (3D) solids [1]. For the latter, the interpretation of spectra of the inelastically scattered electrons traditionally relies on the concept of the energy-loss functions, such as $-\mathrm{Im}\, 1/\epsilon(\mathbf{q},\omega)$ [2], where $\epsilon(\mathbf{q},\omega)$ is the wave-vector and frequency-dependent dielectric function. Other popular loss functions, which came from the field of surface science, are $-\mathrm{Im}\, g(\mathbf{q},\omega)$ and its long-wave limit $-\mathrm{Im}\, 1/[\epsilon(\omega)+1]$, where $g(\mathbf{q},\omega)$ is the so-called g function [3,4]. Loss functions define absorption in the electronic response of the target system, which causes the probing electrons to lose energy.

The description in terms of loss functions is convenient, since the latter are properties of the target system only, saving us the trouble of considering details of the scattering process. Moreover, doing so is justified, as long as the characteristics of the *elastic* scattering at the crystal lattice change slowly within the energy range of interest, constituting a background to the sharp features of the energy losses due to the *inelastic* scattering at the electronic subsystem of the target. This condition is usually satisfied in the EELS of the bulk solids (films) and surfaces, which has led to the loss-functions formalism becoming generally adopted in the theory, and later, with the emergence of graphene [5], automatically transferred to the field of Q2D materials.

Recent advancements in the understanding of the interaction of projectile electrons with Q2D crystals have, however, revealed that the elastic scattering at these systems is far from changing slowly with the energy. In particular, sharp peaks and dips in the energy dependence of the reflection and transmission coefficients were predicted for graphene in the medium (∼10–100 eV) incidence energy range, which were identified as the manifestation of *scattering (diffraction) resonances* (finite-lifetime empty states due to the in-plane and the perpendicular motions coupled by the periodic potential) [6]. Diffraction resonances in graphene have later been confirmed and studied experimentally [7–10]. In this conjunction we also note that resonances in atomic beams scattering from corrugated solid surfaces had been earlier observed [11]. As a consequence, a solid picture of the electron scattering at Q2D crystals becomes impossible without a theory which takes into account all the facets of the probe-target interactions. With such an approach lacking presently, the purpose of this work is to construct the theory of EELS in application to Q2D crystals in the natural terms of the quantum-mechanical scattering of a charge at a many-body system. In this way, all the features of the inelastic and elastic scattering are included, as well as, importantly, the effects of their intermixture. Building this theory, we use the time-dependent density functional theory (TDDFT) [12] to consistently account for the single-particle as well as collective (plasmonic) excitations.

*nazarov@gate.sinica.edu.tw

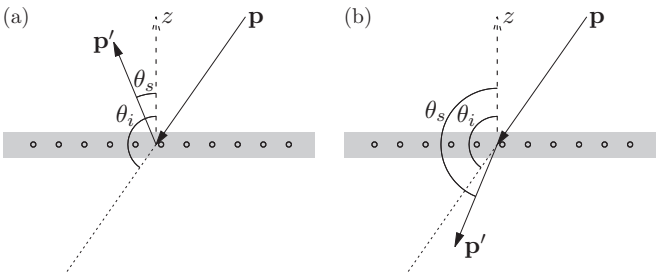

FIG. 1. Illustration of the reflection (a) and transmission (b) geometries of the EELS experiment on a Q2D crystal.

II. METHOD

We are concerned with the EELS experiment as schematized in Fig. 1 for both the reflection and transmission regimes. The starting point of our approach is the general formula for the double differential scattering cross section of a probe electron at the electronic subsystem of a target, accompanied by the elastic scattering at the target's crystal potential. This formula, in the real-space representation, reads [13–15]

$$\frac{d^2\sigma}{d\omega d\Omega}(\mathbf{p}' \leftarrow \mathbf{p}) = -\frac{16\pi^3 p'}{p}\mathrm{Im}\int \frac{\rho^*(\mathbf{r})}{|\mathbf{r}-\mathbf{r}_1|} \times \chi(\mathbf{r}_1,\mathbf{r}_1',\omega)\frac{\rho(\mathbf{r}')}{|\mathbf{r}_1'-\mathbf{r}'|}d\mathbf{r}d\mathbf{r}'d\mathbf{r}_1 d\mathbf{r}_1'. \tag{1}$$

In Eq. (1), χ is the interacting-electrons density response function of the target system, $\mathbf{p}$ and $\mathbf{p}'$ are the momenta of the probing electron before and after the scattering, respectively, $\omega = (p^2 - p'^2)/2$ is the energy transferred to the target,

$$\rho(\mathbf{r}) = \langle \mathbf{r}|\mathbf{p}^+\rangle^* \times \langle \mathbf{r}\,|\mathbf{p}'^-\rangle \tag{2}$$

is the complex-valued "charge density" determined by the elastically scattered waves $|\mathbf{p}^\pm\rangle$, which are solutions to the Lippmann-Schwinger equations [16]

$$|\mathbf{p}^\pm\rangle = |\mathbf{p}\rangle + G^0\left(\frac{p^2}{2} \pm i0_+\right)V^c|\mathbf{p}^\pm\rangle, \tag{3}$$

$\langle \mathbf{r}|\mathbf{p}\rangle = (2\pi)^{-3/2}e^{i\mathbf{p}\cdot\mathbf{r}}$ is plane wave, $V^c(\mathbf{r})$ is the crystal potential, $G^0(E) = (E - \hat{H}_0)^{-1}$ and $\hat{H}_0 = -\frac{1}{2}\Delta + V^c(\mathbf{r})$ are the noninteracting Green's function and the Hamiltonian, respectively, and 0_+ is an infinitesimal positive. Equations (1)–(3) solve the inelastic scattering problem at an arbitrary many-electron system with the interaction between the probe charge and the electronic subsystem of the target accounted for in the first Born approximation, while the probe-lattice interaction is included nonperturbatively [13] (distorted-wave approximation [16]). We note that Eqs. (1)–(3) account for both the long- and short-range (dipole and impact [4], respectively) scattering regimes as the two specific cases.

To make a connection to the pre-TDDFT literature on the inelastic diffraction [17–21] based on the concept of the mixed dynamic form factor (MDFF) [17], we note that (i) Eq. (1) can be also written in terms of MDFF rather than χ. Although the two forms are equivalent, expression via χ is of paramount importance to us, allowing one to invoke the linear-response TDDFT, for which χ is the key quantity [12] and (ii) For 3D crystals, Eqs. (1)–(3) reduce to the results of Ref. [20], but their applicability is broader, permitting, in particular, their use in the Q2D case, in the Laue [see Eq. (6)], rather than Bloch functions representation.

To make a connection to the loss-function formalism, we note that, if the elastic scattering is neglected, meaning that only the first term in the right-hand side of Eq. (3) is kept, Eq. (2) gives $\rho(\mathbf{r}) = e^{i(\mathbf{p}'-\mathbf{p})\cdot\mathbf{r}}/(2\pi)^3$, and Eq. (1) integrates to

$$\frac{d^2\sigma}{d\omega d\Omega}(\mathbf{p}' \leftarrow \mathbf{p}) = -\frac{32\pi^2 p'}{|\Delta\mathbf{p}|^4 p}\mathrm{Im}\,\chi(\Delta\mathbf{p},\Delta\mathbf{p},\omega), \tag{4}$$

where $\Delta\mathbf{p} = \mathbf{p} - \mathbf{p}'$, and χ is written in the reciprocal space representation. If the target is a bulk solid, then the usual bulk energy-loss function $-\mathrm{Im}\,1/\epsilon(\Delta\mathbf{p},\omega)$ is readily retrieved from the right-hand side of Eq. (4). On the other hand, for a Q2D crystal, Eq. (4) coincides (to a coefficient) with the loss function of Ref. [1] in the transmission geometry (see Appendix A for the connection to the g function of surface scattering).

Returning to the simultaneous inelastic and elastic scattering, we note that, in a Q2D crystal, the in-plane component of the wave vector conserves to within a reciprocal lattice vector $\mathbf{G}$. As a consequence, the density response function becomes a matrix in the reciprocal lattice vectors $\chi_{\mathbf{G}\mathbf{G}'}(z,z',\mathbf{q},\omega)$, where the in-plane wave vector $\mathbf{q}$ belongs to the first Brillouin zone. Equation (1) is then conveniently transformed to

$$\begin{aligned}\frac{1}{A}\frac{d\sigma}{d\omega d\Omega}(\mathbf{p}' \leftarrow \mathbf{p}) &= -\frac{64\pi^5 p'}{p}\mathrm{Im}\sum_{\substack{\mathbf{G}\tilde{\mathbf{G}}\\ \mathbf{G}'\tilde{\mathbf{G}}'}}\int \chi_{\mathbf{G}\mathbf{G}'}(z_1,z_1',\mathbf{q},\omega) \\ &\times \frac{e^{-|\mathbf{G}+\mathbf{q}||z_1-z|}e^{-|\mathbf{G}'+\mathbf{q}||z_1'-z'|}}{|\mathbf{G}+\mathbf{q}||\mathbf{G}'+\mathbf{q}|} \\ &\times a^{+*}_{\mathbf{p},\mathbf{G}+\tilde{\mathbf{G}}}(z)a^{-}_{\mathbf{p}',\tilde{\mathbf{G}}+\mathbf{G}_0}(z)a^{+}_{\mathbf{p},\mathbf{G}'+\tilde{\mathbf{G}}'}(z')a^{-*}_{\mathbf{p}',\tilde{\mathbf{G}}'+\mathbf{G}_0} \\ &\times (z')dzdz'dz_1dz_1',\end{aligned} \tag{5}$$

where $a^\pm_{\mathbf{p},\mathbf{G}}(z)$ are the Fourier coefficients in the expansion (Laue representation [22])

$$\langle \mathbf{r}|\mathbf{p}^\pm\rangle = \sum_{\mathbf{G}} a^\pm_{\mathbf{p},\mathbf{G}}(z)e^{i(\mathbf{G}+\mathbf{p}_\parallel)\cdot\mathbf{r}_\parallel}, \tag{6}$$

A is the normalization area, and $\mathbf{G}_0$ reduces the parallel component of the transferred momentum to the first Brillouin zone: $\mathbf{p}_\parallel - \mathbf{p}'_\parallel = \mathbf{q} + \mathbf{G}_0$.

A practical implementation of the approach based on Eq. (5) includes solving the following subproblems:

(1) Calculation of the interacting density response function χ of the Q2D crystal. This is done within the framework of TDDFT with the use of the equality

$$\chi^{-1} = \chi_s^{-1} - f_H - f_{xc}, \tag{7}$$

where χ_s is the independent-electrons [Kohn-Sham (KS)] density response function, and f_H and f_{xc} are the Hartree and the exchange-correlation (xc) kernels, respectively [12].

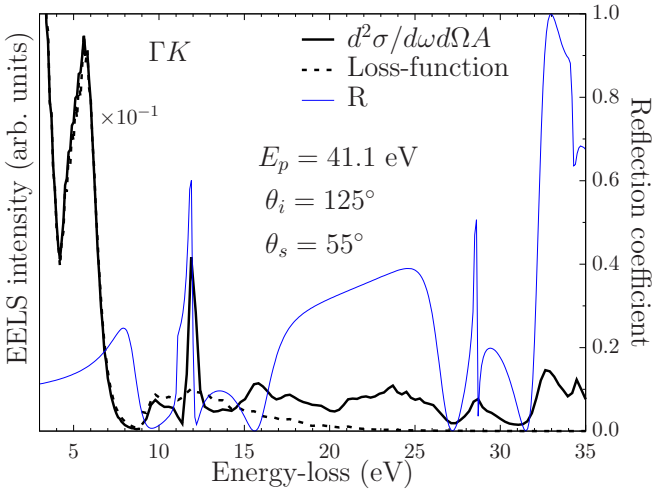

FIG. 2. Calculated EEL reflection spectrum of monolayer graphene [thick black line: Eq. (5)], the one calculated with the use of the surface loss function [dashed line: Appendix A, Eq. (A3)], and the coefficient of reflection (thin blue line plotted against the right y axis). For better visualization, EEL spectra are split into two parts, the low-energy one scaled by 0.1.

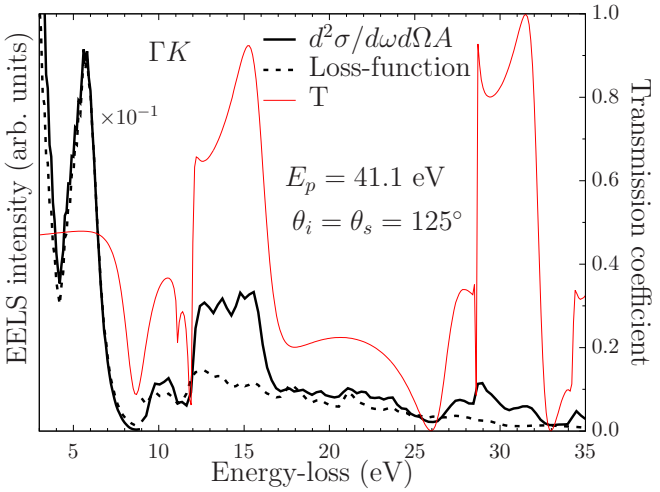

FIG. 3. Calculated EEL transmission spectrum of monolayer graphene [thick line: Eq. (5)], the one calculated with the use of the loss function [dashed line: Eq. (4)], and the coefficient of transmission.

(2) Calculation of the elastic scattering wave functions $|\mathbf{p}^{\pm}\rangle$ of the probe electron by solving Eqs. (3). In other words, the z-dependent coefficients $a^{\pm}_{\mathbf{p},\mathbf{G}}(z)$ in Eq. (6) must be found.

(3) Since the supercell method (substituting the Q2D crystal with an infinite periodic array of such crystals) is used for a practicable solution of the subproblems (1) and (2), the construction of the quantities pertinent to the single Q2D system from those of their array is necessary. For the density response function χ, we use the method of the elimination of the interaction between the fictitious copies of the Q2D crystal [1]. To find the elastic wave functions, we first solve the band-structure problem of the array system, then we construct $|\mathbf{p}^{\pm}\rangle$ of the single Q2D crystal by imposing the proper asymptotic in vacuum (see Appendix B). These conditions ensure $|\mathbf{p}^{+}\rangle$ and $|\mathbf{p}^{-}\rangle$ to be the low-energy electron diffraction (LEED) and the time-reversed LEED wave functions, respectively, of the single Q2D crystal [23].

Our calculations use the local-density approximation (LDA) for the ground-state KS problem [24] and the random-phase approximation (RPA) [setting $f_{xc} = 0$ in Eq. (7)] for the dynamic response. The projectile electron is considered to experience the same potential as electrons of the target.

III. RESULTS AND DISCUSSION

First, we present results corresponding to the experimental setup of the high-resolution EELS (HREELS) [3]. In Fig. 2, the reflection EEL spectrum of graphene calculated with the use of the present theory is plotted together with the reflection coefficient (the latter changing with $\mathbf{p}'$, while $\mathbf{p}$ is fixed). The energy of the incident electrons is $E_p = 41.1$ eV, the angle of incidence is $\theta_i = 125°$, and the angle of scattering is $\theta_s = 55°$ (polar angles are relative to the positive z axis; see Fig. 1). A strong peak of the π plasmon ($\sim$5.6 eV at our geometry) is almost unaffected by the elastic scattering. It is, however, instructive how the influence of the elastic scattering changes the spectrum in the energy range of the $\pi + \sigma$ plasmon, the latter extending broadly from about 10 to 25 eV within the energy-loss function approach [1]. A sharp peak in the reflection coefficient due to the diffraction resonance [6] at $\sim$11.9 eV leads to a peak in the EELS intensity at this energy. The same happens at $\sim$28.5 and 33 eV. Generally, the EEL spectrum becomes a product of the interplay of the inelastic and elastic processes. At the same time, it would be an oversimplification to conclude that the EEL spectrum just follows the reflectance: In Eq. (5) the reflectance coefficient does not factorize and, therefore, the influence of the elastic scattering on the EELS is not straightforward. This can be observed in Fig. 2, considering a maximum in the EEL spectrum at $\sim$15.7 eV, where reflectance has a minimum.

Similar observations can be made from the EELS in the transmission geometry in comparison with the coefficient of transmission, as presented in Fig. 3. We conclude that the elastic scattering affects the EEL spectra dramatically, especially so in the region of the $\pi + \sigma$ plasmon and at higher energies. Different parts of the spectra are strongly enhanced and suppressed in the reflection and transmission regimes, which is mainly due to the presence of the diffraction resonances. The same conclusions are supported by the spectra of the bilayer graphene (see Appendix C).

HREEL experimental spectra of the freestanding graphene are not, to the best of our knowledge, available in the literature so far. Although measurements on graphene supported on substrates have been reported [25–27], a substrate may affect both the diffraction resonances and the electronic response, making impossible the quantitative comparison with the theory of the freestanding graphene. On the other hand, inclusion of a substrate in the *ab initio* theory is a very challenging task, remaining a matter of the future. For the discussion in conjunction with experiment we, therefore, turn to the EELS in the transmission electron microscope (TEM) [28].

EELS measurements on freestanding 2D materials are conducted in TEM using energetic ($\sim$40–120 keV) incident electron beams [28–31]. For energies that high, it is practically

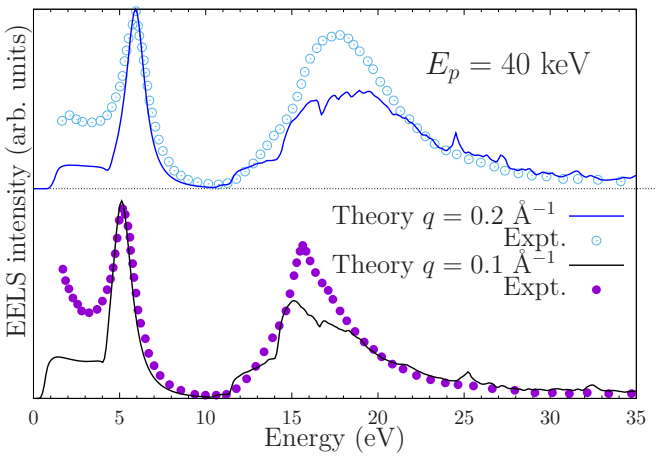

FIG. 4. Calculated EEL spectrum of monolayer graphene (solid lines) and the experimental EELS in TEM (circles). Experimental data are digitized from Ref. [30].

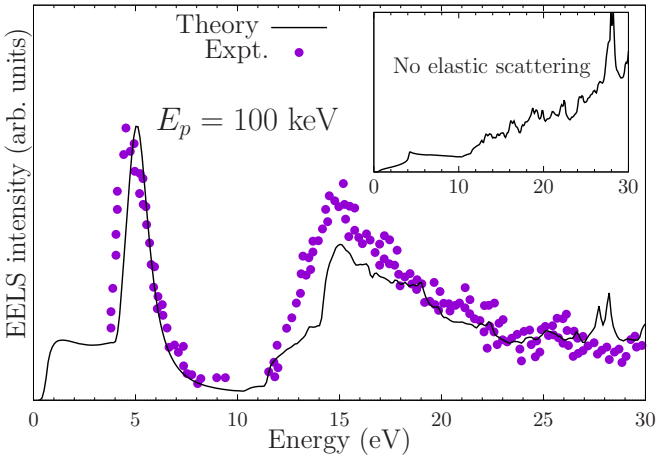

FIG. 5. Calculated EEL spectrum of monolayer graphene (solid line) and the experimental EELS in TEM (circles). Experimental data are of Ref. [29] (digitized from Ref. [32]). Inset shows the spectrum calculated using the loss function of Eq. (4) (neglect of the elastic scattering).

impossible to obtain $|\mathbf{p}^{\pm}\rangle$ of Eq. (3) from the band-structure calculation, but, fortunately, this is also unnecessary, since, in this case, the first Born approximation should already provide an accurate solution to the elastic scattering problem. We therefore use Eq. (5) again, but with the coefficients $a^{\pm}_{\mathbf{p},\mathbf{G}}(z)$ found to the first order in the magnitude of $V^c(\mathbf{r})$ (see Appendix D).

Diffraction resonances do not exist or are negligible in the keV energy range, and the influence of the elastic scattering on the inelastic one differs for EELS in TEM from that for HREELS, while, as we will show, it still remains important. The results of our calculations presented in Fig. 4 correspond to the setup and are compared to the experiment of Ref. [30]. The geometry of this experiment suggests that the transferred in-plane momentum $\Delta\mathbf{p}_\parallel$ belongs to the first Brillouin zone. As a consequence (in the absence of diffraction resonances), the full calculation with the use of Eq. (5) results in a spectrum indistinguishable from that obtained with Eq. (4) for the energy-loss function (not shown). On the other hand, in Fig. 5 we plot results corresponding to the celebrated EELS in TEM experiment of Ref. [29]. Analysis of the geometry in this case shows that $|\Delta\mathbf{p}_\parallel| \approx 3.08$ Å^{-1}, which is outside the first Brillouin zone of graphene. The calculated spectrum ignoring the influence of the elastic scattering [obtained by Eq. (4)] is plotted in the inset of Fig. 5, and it clearly bears no resemblance to the experimental spectrum. This can be understood considering that, if the elastic channel is switched off, the whole (huge) momentum $\Delta\mathbf{p}_\parallel$ must be absorbed by the electronic subsystem, resulting in excitations in higher bands. Although such processes do take place, their contribution to the spectrum is negligible when the elastic scattering is taken into account, which restores a reasonable agreement with experiment, as can be seen in the main panel of Fig. 5. The elastic channel accepts the reciprocal-lattice-vector part of the momentum, with the rest absorbed by the electronic subsystem. We emphasize that the above being a reasoning in physical terms, our Eq. (5) includes all the processes in question, producing correct results automatically, without any by-hand operations (cf. Ref. [32], where the reciprocal lattice vector is subtracted implicitly).

As noted above, this work uses the LDA to the DFT for the ground state and RPA for the dynamic response calculations, respectively. This is done consciously for the sake of simplicity and considering that our goal is highlighting the coupling between the inelastic and elastic processes, rather than studying the many-body effects in Q2D materials, the latter problem having been addressed in a large body of literature (see, e.g., Ref. [33], and references therein). The basis of our approach, Eq. (5), remains, however, valid at any level of (TD)DFT, allowing future inclusion of the many-body effects in the framework of this theory. At the same time, it must be noted that the supercell method might encounter difficulties in the presence of the long-range xc [34], in which case the "native" approaches [35] (considering a single Q2D crystal from the very beginning) will be necessary. The well-known shortcomings of LDA and RPA [36] are the likely source of the remaining discrepancies between our calculations and the experiment in the energy range of the $\pi + \sigma$ plasmon (see Appendix E for further discussion).

IV. CONCLUSIONS

We have identified fundamental limitations in the conventional picture of the inelastic scattering of electrons at quasi-two-dimensional crystalline systems. That is the neglect of the simultaneous *potential scattering* at the lattice, which turns out to be critically important in the energy range of incident electrons of $\sim$10–100 eV, corresponding to the setup of the high-resolution EELS. We have overcome this problem by constructing the theory of the one-step combined inelastic and elastic electron scattering at Q2D crystals. These results open a path to the *theoretically interpretable* use of HREELS for studying Q2D materials with the meV resolution, the latter unachievable with EELS in TEM.

In illustrative calculations, a strong coupling between the inelastic and elastic channels has been found in graphene

in the HREELS regime. In particular, the excitation of the $\pi+\sigma$ plasmon is dramatically affected by the scattering in the elastic channel. These theoretical findings constitute a strong motivation for performing HREELS experiments on freestanding Q2D crystals, especially so in view of the recent advances in the HREELS technique [37]. For EELS in TEM, our theory elucidates the absorbed momenta distribution between plasmon excitation and diffraction. By this, a reasonable agreement between the theory and the experimental EELS in TEM has been observed for graphene.

We, finally, argue that, overcoming the limitations of the energy-loss functions formalism, our approach can be expected to replace it as a standard theoretical tool in the EELS of mesoscopic crystals.

ACKNOWLEDGMENTS

The authors are grateful to Dr. Ming-Wen Chu for providing the digital EELS experimental data of Ref. [31]. This work was supported by the Ministry of Science and Technology, Taiwan (Projects No. 105–2112–M–001–010 and No. 106–2112–M–001–021) and by the Spanish Ministry of Economy and Competitiveness MINECO (Project No. FIS2016-76617-P).

APPENDIX A: CONNECTION TO THE DIPOLE-SCATTERING REGIME

Here for simplicity, we consider the flat in-plane potential and, therefore, we can rewrite Eq. (5) with all the reciprocal lattice vectors equated to zero:

$$\frac{1}{A}\frac{d\sigma}{d\omega d\Omega}(\mathbf{p}'\leftarrow\mathbf{p}) = -\frac{64\pi^5 p'}{pq^2}\mathrm{Im}\int \chi(z_1,z_1',\mathbf{q},\omega)e^{-q|z_1-z|}e^{-q|z_1'-z'|}a_{\mathbf{p}}^{+*} \times(z)a_{\mathbf{p}'}^{-}(z)a_{\mathbf{p}}^{+}(z')a_{\mathbf{p}'}^{-*}(z')dzdz'dz_1dz_1'. \quad \text{(A1)}$$

The dipole-scattering regime is the one when the target is excited through the long-range Coulomb interaction with a probe, without the probe charge entering the electron density of the target. Assuming that the electron density of the target and the incident and reflected probe are separated by the $z=0$ plane, we can consider that $\chi(z_1,z_1',\mathbf{q},\omega)$ is nonzero only when both z_1 and z_1' are negative, but $a_{\mathbf{p}}^{\pm}(z)$ are nonzero only if z is positive. Then Eq. (A1) can be rewritten as

$$\frac{1}{A}\frac{d\sigma}{d\omega d\Omega}(\mathbf{p}'\leftarrow\mathbf{p}) = -\frac{64\pi^5 p'}{pq^2}\mathrm{Im}\int \chi(z_1,z_1',\mathbf{q},\omega)e^{-q(z-z_1)}e^{-q(z'-z_1')} \times a_{\mathbf{p}}^{+*}(z)a_{\mathbf{p}'}^{-}(z)a_{\mathbf{p}}^{+}(z')a_{\mathbf{p}'}^{-*}(z')dzdz'dz_1dz_1', \quad \text{(A2)}$$

which further reduces to

$$\frac{1}{A}\frac{d\sigma}{d\omega d\Omega}(\mathbf{p}'\leftarrow\mathbf{p}) = -\frac{64\pi^5 p'}{pq^2}\mathrm{Im}\int \chi(z,z',\mathbf{q},\omega)e^{q(z+z')}dzdz' \times\left|\int e^{-qz}a_{\mathbf{p}}^{+*}(z)a_{\mathbf{p}'}^{-}(z)dz\right|^2. \quad \text{(A3)}$$

We see that the differential cross section factorizes in this case into the product of two terms. The first,

$$-\mathrm{Im}g(\mathbf{q},\omega) = -\mathrm{Im}\int \chi(z,z',\mathbf{q},\omega)e^{q(z+z')}dzdz', \quad \text{(A4)}$$

is a characteristic of the target only, and it exactly coincides with the minus imaginary part of the g function [1,4]. The second term in Eq. (A3) is a purely kinematic factor, depending on the motion of the probe only.

APPENDIX B: LEED WAVE FUNCTIONS' ASYMPTOTIC BOUNDARY CONDITIONS IN VACUUM

The asymptotic behavior of $\langle\mathbf{r}|\mathbf{p}^{\pm}\rangle$ and, hence, that of $a_{\mathbf{p},\mathbf{G}}^{\pm}(z)$, follows from Eqs. (3). Introducing the notation

$$k_{\mathbf{G}} = \sqrt{p_z^2-\mathbf{G}^2-2\mathbf{G}\cdot\mathbf{p}_{\parallel}+i0_+}, \quad \mathrm{Im}\,k_{\mathbf{G}}>0, \quad \text{(B1)}$$

we can easily find at $k_{\mathbf{G}}^2\geqslant 0$,

$$a_{\mathbf{p},\mathbf{G}}^{\pm}(z) = \delta_{\mathbf{G}\mathbf{0}}e^{ip_z z}+\begin{cases} b_{\mathbf{p},\mathbf{G}}^{\pm}e^{\pm ik_{\mathbf{G}}z}, & z\to\infty \\ c_{\mathbf{p},\mathbf{G}}^{\pm}e^{\mp ik_{\mathbf{G}}z}, & z\to-\infty. \end{cases} \quad \text{(B2)}$$

Otherwise, if $k_{\mathbf{G}}^2<0$,

$$a_{\mathbf{p},\mathbf{G}}^{\pm}(z) = \begin{cases} b_{\mathbf{p},\mathbf{G}}^{\pm}e^{-|k_{\mathbf{G}}|z}, & z\to\infty \\ c_{\mathbf{p},\mathbf{G}}^{\pm}e^{|k_{\mathbf{G}}|z}, & z\to-\infty. \end{cases} \quad \text{(B3)}$$

APPENDIX C: EEL SPECTRA OF BILAYER GRAPHENE

EEL spectra of bilayer graphene in the reflection and transmission modes are presented in Fig. 6 and 7, respectively.

APPENDIX D: LEED WAVE FUNCTIONS IN THE FIRST BORN APPROXIMATION

From Eqs. (3) we can write to the first order in V^c

$$|\mathbf{p}^{+}\rangle = \left[1+G^0\left(\frac{p^2}{2}+i0_+\right)V^c\right]|\mathbf{p}\rangle. \quad \text{(D1)}$$

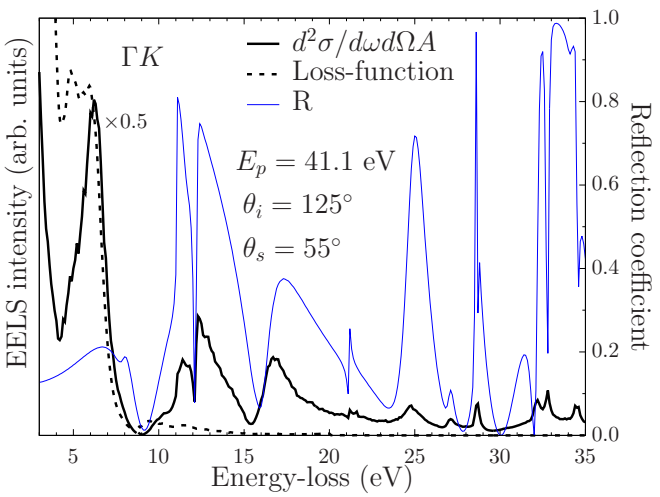

FIG. 6. Calculated EEL reflection spectrum of bilayer graphene (thick black line), loss function (dashed line), and the coefficient of reflection (blue). In contrast to the monolayer case, π plasmon is influenced too by the inclusion of the elastic scattering.

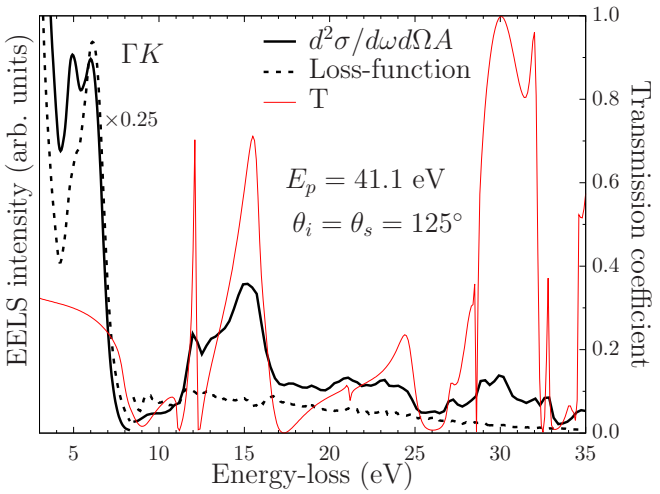

FIG. 7. Calculated EEL transmission spectrum of bilayer graphene (thick black line), loss function (dashed lines), and the coefficient of transmission (red). In contrast to the monolayer case, π plasmon is influenced too by the inclusion of the elastic scattering.

We use the Fourier-series representation of the potential within the interval $z \in [-\frac{D}{2}, \frac{D}{2}]$, outside of which it is zero,

$$V^c(\mathbf{r}) = \Omega_D(z) \sum_{\mathbf{G},g} V_{\mathbf{G},g} e^{i(\mathbf{G}\cdot\mathbf{r}_\parallel + gz)}, \tag{D2}$$

where $g = 2\pi n/D$, $n = 0, \pm 1, \ldots$, and

$$\Omega_D(z) = \begin{cases} 1, & |z| \leqslant D/2 \\ 0, & |z| > D/2. \end{cases} \tag{D3}$$

Expanding (D2) into the Fourier integral on $z \in (-\infty, \infty)$, we have

$$V^c(\mathbf{r}) = \int \frac{dg'}{2\pi i g'} \sum_{\mathbf{G},g} V^c_{\mathbf{G},g} e^{i\mathbf{G}\cdot\mathbf{r}_\parallel} e^{i(g+g')z} [e^{ig'D/2} - e^{-ig'D/2}]. \tag{D4}$$

Substituting Eq. (D4) into (D1) and applying G^0 explicitly, we have

$$\langle \mathbf{r}|\mathbf{p}^+\rangle = \frac{1}{(2\pi)^{3/2}} \left\{ e^{i\mathbf{p}\cdot\mathbf{r}} - \sum_{\mathbf{G},g} V^c_{\mathbf{G},g} e^{i(\mathbf{G}+\mathbf{p}_\parallel)\cdot\mathbf{r}_\parallel} \int \frac{dg'}{\pi i g'} \frac{e^{i(g+p_z)z}[e^{ig'(z+D/2)} - e^{ig'(z-D/2)}]}{(g'+g+p_z)^2 - (p_z^2 - \mathbf{G}^2 - 2\mathbf{G}\cdot\mathbf{p}_\parallel + i0_+)} \right\}. \tag{D5}$$

After an explicit integration, we have separately in the three regions

$$\langle \mathbf{r}|\mathbf{p}^+\rangle = \frac{1}{(2\pi)^{3/2}} \left\{ e^{i\mathbf{p}\cdot\mathbf{r}} - 2i \sum_{\mathbf{G},g} V^c_{\mathbf{G},g} e^{i(\mathbf{G}+\mathbf{p}_\parallel)\cdot\mathbf{r}_\parallel} \frac{e^{ik_\mathbf{G} z} e^{igD/2} \sin[(k_\mathbf{G} - p_z)D/2]}{(k_\mathbf{G} - g - p_z)k_\mathbf{G}} \right\}, \quad z > D/2, \tag{D6}$$

$$\langle \mathbf{r}|\mathbf{p}^+\rangle = \frac{1}{(2\pi)^{3/2}} \left\{ e^{i\mathbf{p}\cdot\mathbf{r}} - 2i \sum_{\mathbf{G},g} V^c_{\mathbf{G},g} e^{i(\mathbf{G}+\mathbf{p}_\parallel)\cdot\mathbf{r}_\parallel} \frac{e^{-ik_\mathbf{G} z} e^{igD/2} \sin[(k_\mathbf{G} + p_z)D/2]}{(k_\mathbf{G} + g + p_z)k_\mathbf{G}} \right\}, \quad z < -D/2. \tag{D7}$$

$$\langle \mathbf{r}|\mathbf{p}^+\rangle = \frac{1}{(2\pi)^{3/2}} \left\{ e^{i\mathbf{p}\cdot\mathbf{r}} - \sum_{\mathbf{G},g} V^c_{\mathbf{G},g} e^{i(\mathbf{G}+\mathbf{p}_\parallel)\cdot\mathbf{r}_\parallel} \left[\frac{2e^{i(g+p_z)z}}{(g+p_z)^2 - k_\mathbf{G}^2} + \frac{e^{ik_\mathbf{G} z} e^{i(k_\mathbf{G} - g - p_z)D/2}}{(k_\mathbf{G} - g - p_z)k_\mathbf{G}} + \frac{e^{-ik_\mathbf{G} z} e^{i(k_\mathbf{G} + g + p_z)D/2}}{(k_\mathbf{G} + g + p_z)k_\mathbf{G}} \right] \right\}, \quad |z| < D/2, \tag{D8}$$

where $k_\mathbf{G}$ is defined by Eq. (B1). Therefore, with the use of Eq. (6),

$$a^+_{\mathbf{p},\mathbf{G}}(z) = \frac{1}{(2\pi)^{3/2}} \left\{ e^{ip_z z}\delta_{\mathbf{G}\mathbf{0}} - 2i \sum_g V^c_{\mathbf{G},g} \frac{e^{ik_\mathbf{G} z} e^{igD/2} \sin[(k_\mathbf{G} - p_z)D/2]}{(k_\mathbf{G} - g - p_z)k_\mathbf{G}} \right\}, \quad z > D/2, \tag{D9}$$

$$a^+_{\mathbf{p},\mathbf{G}}(z) = \frac{1}{(2\pi)^{3/2}} \left\{ e^{ip_z z}\delta_{\mathbf{G}\mathbf{0}} - 2i \sum_g V^c_{\mathbf{G},g} \frac{e^{-ik_\mathbf{G} z} e^{igD/2} \sin[(k_\mathbf{G} + p_z)D/2]}{(k_\mathbf{G} + g + p_z)k_\mathbf{G}} \right\}, \quad z < -D/2. \tag{D10}$$

$$a^+_{\mathbf{p},\mathbf{G}}(z) = \frac{1}{(2\pi)^{3/2}} \left\{ e^{ip_z z}\delta_{\mathbf{G}\mathbf{0}} - \sum_g V^c_{\mathbf{G},g} \left[\frac{2e^{i(g+p_z)z}}{(g+p_z)^2 - k_\mathbf{G}^2} + \frac{e^{ik_\mathbf{G} z} e^{i(k_\mathbf{G} - g - p_z)D/2}}{(k_\mathbf{G} - g - p_z)k_\mathbf{G}} + \frac{e^{-ik_\mathbf{G} z} e^{i(k_\mathbf{G} + g + p_z)D/2}}{(k_\mathbf{G} + g + p_z)k_\mathbf{G}} \right] \right\}, \quad |z| < D/2. \tag{D11}$$

Finally, since $|\mathbf{p}^-\rangle = |(-\mathbf{p})^+\rangle^*$, $a^-_{\mathbf{p},\mathbf{G}}(z)$ are found as

$$a^-_{\mathbf{p},\mathbf{G}}(z) = a^+_{-\mathbf{p},-\mathbf{G}}(z)^*. \tag{D12}$$

APPENDIX E: FURTHER COMPARISON WITH EXPERIMENT

Although theoretical spectra in Figs. 4 and 5 are in qualitative agreement with the experimental EELS in TEM, two differences can be noticed. First, in Fig. 4 in the energy

range below the π-plasmon peak, the intensities of the experimental spectra are greater than those of the theoretical ones. We attribute this to the finite momentum resolution ($\Delta q = 0.1\,\text{Å}^{-1}$) in the experiment [30]. Indeed, the growth of the intensity with the decreasing energy below the π peak is characteristic for smaller wave vectors [30] (see also Fig. 8). Because of the contribution from the smaller q's than the nominal one, this leads to the discrepancy between the theory and experiment in this energy range.

Secondly, the experimental $\pi + \sigma$ plasmon is well reproduced by our calculations except for the amplitude around the maxima. This feature is persistent with respect to the change of q and, therefore, is likely to be related to the shortcomings of the LDA and RPA used in the calculations.

Finally, in Fig. 8 we present theoretical spectra in comparison with the recent experimental EELS in TEM at very small wave vectors [31]. At so small q's, the theoretical π peak in pristine graphene is almost dispersionless in LDA and RPA, which is due to the overlapping of the plasmon with the interband transitions [1]. This finds itself in contrast with the experimental behavior [31]. The inclusion of the static exchange and correlations beyond the LDA and going beyond RPA by accounting for the *dynamic* exchange and correlation with the use of f_{xc} in Eq. (7) of a sufficient degree of sophistication, may be the way to resolve this discrepancy.

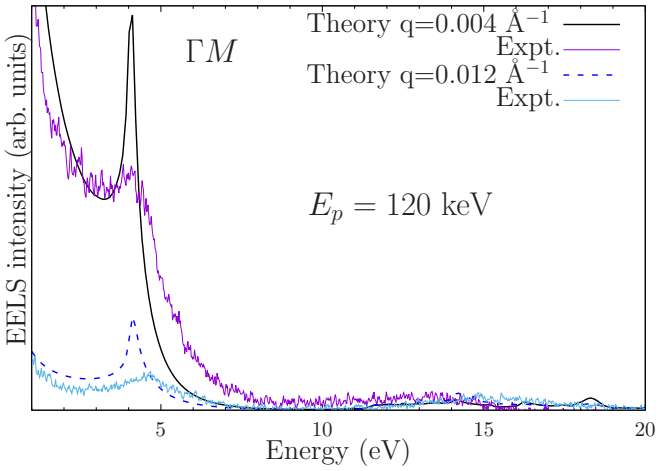

FIG. 8. Calculated EEL spectrum of graphene (smooth solid lines) and the experimental EELS in TEM (noisy lines). Experimental data are from Ref. [31].

[1] V. U. Nazarov, Electronic excitations in quasi-2D crystals: What theoretical quantities are relevant to experiment? New J. Phys. **17**, 073018 (2015).

[2] D. Pines and P. Nozieres, *The theory of quantum liquids* (Benjamin, New York, 1966).

[3] H. Ibach and D. L. Mills, *Electron energy loss spectroscopy and surface vibrations* (Academic, New York, 1982).

[4] A. Liebsch, *Electronic excitations at metal surfaces* (Plenum, New York, 1997).

[5] K. S. Novoselov, A. K. Geim, S. V. Morozov, D. Jiang, Y. Zhang, S. V. Dubonos, I. V. Grigorieva, and A. A. Firsov, Electric field effect in atomically thin carbon films, Science **306**, 666 (2004).

[6] V. U. Nazarov, E. E. Krasovskii, and V. M. Silkin, Scattering resonances in two-dimensional crystals with application to graphene, Phys. Rev. B **87**, 041405(R) (2013).

[7] M. Pisarra, P. Riccardi, A. Sindona, A. Cupolillo, N. Ligato, C. Giallombardo, and L. Caputi, Probing graphene interfaces with secondary electrons, Carbon **77**, 796 (2014).

[8] J. Jobst, J. Kautz, D. Geelen, R. M. Tromp, and S. J. van der Molen, Nanoscale measurements of unoccupied band dispersion in few-layer graphene, Nat. Commun. **6**, 8926 (2015).

[9] F. Wicki, J.-N. Longchamp, T. Latychevskaia, C. Escher, and H.-W. Fink, Mapping unoccupied electronic states of freestanding graphene by angle-resolved low-energy electron transmission, Phys. Rev. B **94**, 075424 (2016).

[10] M. Krivenkov, D. Marchenko, J. Sánchez-Barriga, O. Rader, and A. Varykhalov, Suppression of electron scattering resonances in graphene by quantum dots, Appl. Phys. Lett. **111**, 161605 (2017).

[11] E. Engdahl, N. Moiseyev, and T. Maniv, A theory of He diffraction and resonance scattering from Cu(115) by the complex coordinate method, J. Chem. Phys. **94**, 1636 (1991); E. Engdahl, T. Maniv, and N. Moiseyev, Gas–surface scattering cross section by the complex coordinate method, *ibid.* **94**, 6330 (1991).

[12] E. K. U. Gross and W. Kohn, Local Density-Functional Theory of Frequency-Dependent Linear Response, Phys. Rev. Lett. **55**, 2850 (1985).

[13] V. U. Nazarov, Analytical properties of dielectric response of semi-infinite systems and the surface electron energy loss function, Surf. Sci. **331-333**, 1157 (1995).

[14] V. U. Nazarov, Multipole surface-plasmon-excitation enhancement in metals, Phys. Rev. B **59**, 9866 (1999).

[15] V. U. Nazarov and S. Nishigaki, Inelastic low energy electron diffraction at metal surfaces, Surf. Sci. **482-485**, 640 (2001).

[16] J. R. Taylor, *Scattering theory* (Wiley, New York, 1972).

[17] H. Kohl and H. Rose, in *Advances in electronics and electron physics*, edited by P. W. Hawkes (Academic, New York, 1985), Vol. 65, pp. 173–227.

[18] S. L. Dudarev, L.-M. Peng, and M. J. Whelan, Correlations in space and time and dynamical diffraction of high-energy electrons by crystals, Phys. Rev. B **48**, 13408 (1993).

[19] L. J. Allen and T. W. Josefsson, Inelastic scattering of fast electrons by crystals, Phys. Rev. B **52**, 3184 (1995).

[20] P. Schattschneider, B. Jouffrey, and M. Nelhiebel, Dynamical diffraction in electron-energy-loss spectrometry: The independent Bloch-wave model, Phys. Rev. B **54**, 3861 (1996).

[21] P. Schattschneider, M. Nelhiebel, H. Souchay, and B. Jouffrey, The physical significance of the mixed dynamic form factor, Micron **31**, 333 (2000).

[22] M. v. Laue, The diffraction of an electron-wave at a single layer of atoms, Phys. Rev. **37**, 53 (1931).

[23] V. U. Nazarov, V. M. Silkin, and E. E. Krasovskii, Role of the kinematics of probing electrons in electron energy-loss spectroscopy of solid surfaces, Phys. Rev. B **93**, 035403 (2016).

[24] W. Kohn and L. J. Sham, Self-consistent equations including exchange and correlation effects, Phys. Rev. **140**, A1133 (1965).

[25] J. Lu, K. P. Loh, H. Huang, W. Chen, and A. T. S. Wee, Plasmon dispersion on epitaxial graphene studied using high-resolution electron energy-loss spectroscopy, Phys. Rev. B **80**, 113410 (2009).

[26] A. Politano, A. R. Marino, V. Formoso, D. Farías, R. Miranda, and G. Chiarello, Evidence for acoustic-like plasmons on epitaxial graphene on Pt(111), Phys. Rev. B **84**, 033401 (2011).

[27] A. Cupolillo, A. Politano, N. Ligato, D. M. Cid Perez, G. Chiarello, and L. S. Caputi, Substrate-dependent plasmonic properties of supported graphene, Surf. Sci. **634**, 76 (2015).

[28] R. F. Egerton, Electron energy-loss spectroscopy in the TEM, Rep. Prog. Phys. **72**, 016502 (2009).

[29] T. Eberlein, U. Bangert, R. R. Nair, R. Jones, M. Gass, A. L. Bleloch, K. S. Novoselov, A. Geim, and P. R. Briddon, Plasmon spectroscopy of free-standing graphene films, Phys. Rev. B **77**, 233406 (2008).

[30] P. Wachsmuth, R. Hambach, M. K. Kinyanjui, M. Guzzo, G. Benner, and U. Kaiser, High-energy collective electronic excitations in free-standing single-layer graphene, Phys. Rev. B **88**, 075433 (2013).

[31] S. C. Liou, C.-S. Shie, C. H. Chen, R. Breitwieser, W. W. Pai, G. Y. Guo, and M.-W. Chu, π-plasmon dispersion in free-standing graphene by momentum-resolved electron energy-loss spectroscopy, Phys. Rev. B **91**, 045418 (2015).

[32] V. Despoja, D. Novko, K. Dekanić, M. Šunjić, and L. Marušić, Two-dimensional and π plasmon spectra in pristine and doped graphene, Phys. Rev. B **87**, 075447 (2013).

[33] D. A. Siegel, C.-H. Park, C. Hwang, J. Deslippe, A. V. Fedorov, S. G. Louie, and A. Lanzara, Many-body interactions in quasi-freestanding graphene, Proc. Natl. Acad. Sci. USA **108**, 11365 (2011).

[34] J. F. Dobson, T. Gould, and S. Lebègue, Layer response theory: Energetics of layered materials from semianalytic high-level theory, Phys. Rev. B **93**, 165436 (2016).

[35] P. E. Trevisanutto and G. Vignale, *Ab initio* electronic structure of quasi-two-dimensional materials: A "native" Gaussian-plane wave approach, J. Chem. Phys. **144**, 204122 (2016).

[36] G. F. Giuliani and G. Vignale, *Quantum theory of the electron liquid* (Cambridge University Press, Cambridge, 2005).

[37] S. Vig, A. Kogar, M. Mitrano, A. A. Husain, V. Mishra, M. S. Rak, L. Venema, P. D. Johnson, G. D. Gu, E. Fradkin, M. R. Norman, and P. Abbamonte, Measurement of the dynamic charge response of materials using low-energy, momentum-resolved electron energy-loss spectroscopy (M-EELS), SciPost Phys. **3**, 026 (2017).